Superconductivity in layered Nb/Gd films

C. Strunk, C. Sürgers, U. Paschen, and H. v. Löhneysen
Physikalisches Institut, Universität Karlsruhe, D-76128 Karlsruhe, Germany
(Received 9 August 1993)

The transition temperature and the critical fields of electron-beam evaporated Nb/Gd/Nb triple layers and Nb/Gd multilayers have been determined by measurements of the electrical resistivity and the dc susceptibility. For constant thickness d_{Gd} of the Gd layers, we observe a decrease of T_c and $H_{c2\perp}$ with decreasing thickness d_{Nb} of Nb layers down to a critical thickness d_c, below which superconductivity is completely destroyed. The parallel critical fields mostly show the square-root temperature dependence near T_c, typical for two-dimensional superconductors. As predicted theoretically, competing pair-breaking mechanisms lead to a nonmonotonic dependence of $H_{c\parallel}$ on d_{Nb}. We have also studied the dependence $T_c(d_{Gd})$ with constant d_{Nb} and find a decrease of the $T_c(d_{Gd})$ curve with increasing d_{Gd} and a steplike structure at $d_{Gd}\approx 20$ Å. To clarify the nature of this step, the ferromagnetic transition of the Gd films is determined with the transverse magneto-optical Kerr effect. Long-range magnetic order is found only above $d_{Gd}\approx 20$ Å, which is attributed to the formation of a discontinuous film below this thickness. These results indicate a change in the underlying pair-breaking mechanism.

I. INTRODUCTION

Since the 1960's the interaction between superconductivity (SC) and ferromagnetism (FM) has attracted considerable interest. Because (conventional) SC requires a coupling between electron pairs with antiparallel spin, whereas FM favors a parallel alignment of electron spins through the FM exchange field, both mechanisms are counteractive. Usually, the FM state has a higher stability and therefore tends to suppress the Cooper pairing.

In one line of approach the possible coexistence of both phenomena in bulk samples has been examined. The first theories considering the effect of an FM exchange field have been proposed by Fulde and Ferrell and independently by Larkin and Ovchinnikov.[1] They obtained an unorthodox SC state with a spatially modulated order parameter. The Fulde-Ferrell-Larkin-Ovchinnikov (FFLO) state should be possible if the Zeeman splitting of the conduction-electron bands—either caused by an exchange field or an external magnetic field—makes the usual Cooper pairing unfavorable. An additional requirement for the existence of the FFLO state is that SC should not be destroyed by the orbital effect of the magnetic field, i.e., H_{c2} has to be large. In conventional SC this can be achieved through a short electron mean free path. Unfortunately, in contrast to a homogeneous SC state, the FFLO phase turned out to be very sensitive to elastic-scattering events.[2] Therefore, the effect has not been seen in conventional SC up to now. Very recently, experimental evidence for this state has been found in the heavy-fermion SC UPd_2Al_3 (Ref. 3) where the effect was induced by an external magnetic field.

In a second line of approach, the penetration of Cooper pairs into magnetic films via the so-called proximity effect was studied.[4,5] In their classical paper,[4] Hauser, Theurer, and Werthamer investigated the T_c depression in Pb films by thin magnetic overlayers of Fe, Ni, Gd, and Cr. For the interpretation of their data, a combination of the DeGennes-Werthamer (DGWH) theory of the proximity effect with the Abrikosov-Gorkov (AG) model for pair breaking by independent magnetic moments was employed. Although fair agreement between theory and experiment was achieved, the assumption of scattering by independent moments remained unsatisfactory.

Recently, the proximity effect in SC/FM multilayers has been studied theoretically by Radovic *et al.*[6] The authors proposed the formation of a FFLO-like order-parameter profile near the SC/FM boundary. This should cause oscillations of T_c as a function of thickness of the magnetic layers.[7] Furthermore, perpendicular and parallel critical fields have been calculated. Due to competing pair-breaking mechanisms, a nonmonotonic behavior of $H_{c\parallel}$ as a function of the thickness of the SC layer is expected.[8]

In this work, we present a detailed experimental study of Nb/Gd triple layers and multilayers with the aim to search for and investigate the above-mentioned phenomena. We chose niobium as the SC, because due to its high transition temperature a large portion of the phase diagram is observable for temperatures down to 1.5 K. Gadolinium is a ferromagnet with $T_{Curie}(\text{bulk})=292$ K and has the simplest magnetic structure among the rare-earth metals.[9] Epitaxial growth in the Nb/Gd system has been studied in detail before.[10,11] Sharp interfaces without interdiffusion should be obtained, because the two components are not mutually soluble neither in the solid nor in the liquid phase.[12]

This paper is organized as follows. After a short survey of experimental details in Sec. II, the sample preparation and characterization is described in Sec. III. In Sec. IV, the dependence of SC properties on the Nb thickness d_{Nb} is discussed in terms of pair breaking by the proximity effect and by external magnetic fields. A comparison between triple layers and multilayers is given. In Sec. V, we discuss in detail the microscopic origin of the pair breaking by the Gd interlayers which is analyzed in terms of the different theories mentioned above.[4,6] The Gd lay-

0163-1829/94/49(6)/4053(11)/$06.00

ers show a transition from paramagnetic to ferromagnetic behavior with increasing d_{Gd} and therefore allow a comparison of the influence of random and FM ordered spins on the superconductivity. A preliminary report on some of the results presented here is given elsewhere.[13]

II. EXPERIMENTAL DETAILS

The samples were grown at room temperature by electron-beam evaporation on sapphire single crystals with $(11\bar{2}0)$ orientation in a UHV system as described elsewhere.[11] We prepared Nb/Gd multilayers and Nb/Gd/Nb triple layers. In case of the multilayers the top and bottom films consisted of 100-Å Nb to prevent chemical reactions of the top and bottom Gd films with and the substrate, respectively. The oxidation of the upper Nb layer in air is restricted to the first 20 Å.[14] Because of their small thickness the Nb cover layers were not superconducting as will become evident in the following. In the multilayer samples d_{Gd} was kept constant at 34 Å, while d_{Nb} was varied.

For the study of the influence of d_{Gd}, the achieved reproducibility of the quartz monitor thickness for samples prepared in different evaporation processes, turned out to be not sufficient. Therefore, series of 18 triple layers with identical Nb layers but increasing d_{Gd} were prepared in a single run. After deposition of the first Nb layer a sample shutter was opened with constant velocity during the evaporation of Gd, exposing one substrate after the other to the vapor beam. Adjacent samples differed in nominal d_{Gd} by about 2 Å, while d_{Gd} varied within the individual samples by less than $\frac{1}{10}$ of this value. Afterwards, the second Nb layer was evaporated on all samples simultaneously again. By this procedure we obtained constant material parameters of the Nb layers within the series, which is essential for separating the influence of the d_{Gd} and d_{Nb} variations. The influence of the substrate temperature T_S during evaporation on the sample quality was studied systematically.[11,14] Concerning the SC properties, the best results (smallest T_c width) have been obtained at room temperature. At higher T_S the larger mobility of the atoms leads to the formation of islands of Nb on Gd,[11] which give rise to a strong broadening of the SC transition.

Conventional four terminal resistance measurements were performed in a ^{4}He cryostat down to 1.5 K, using a commercial ac resistance bridge (LR400). Leads were attached to the samples with silver paint. The absolute accuracy of the resistivity was about 7%, which is mainly due to the error in the determination of the geometry factor. The SC critical fields were determined from the 50% point of the resistive transition by ramping the magnetic field up until 90% of the resistance value at 10 K was reached and then ramping down again while the temperature was kept constant within typically 2 mK. Both curves showed a ramp-rate dependent shift of typical 10–40 mT, which is due to the shunt resistor in the persistent switch of the SC magnet. Therefore, especially for the determination of small critical fields, very low ramp rates were used. For the resulting field values always the mean of both ramp directions was taken.

To check whether the resistively determined SC transition temperatures were not due to SC percolation paths only, measurements of the dc magnetization have been performed in a superconducting quantum interference device (SQUID) magnetometer with magnetic field perpendicular to the films.[15]

III. SAMPLE CHARACTERIZATION

A. X-ray diffraction

The x-ray-diffraction patterns (Cu $K\alpha$ radiation) at large angles show the Bragg reflections of the different components, i.e., the Nb(110), the Gd(0002), and the sapphire $(11\bar{2}0)$ reflection (Fig. 1). Despite the low substrate temperature, the samples are highly textured, which follows from the absence of other peaks, like the Nb (200) reflection at $\approx 56°$ (not shown in Fig. 1). The broadening of the Gd (0002) reflections and their small height is due to the very small thickness of the Gd layers. In the multilayer samples no satellites of the Bragg peaks are apparent, indicating the formation of a structurally incoherent superlattice.[11] The rocking curves of the Nb (110) Bragg peak consist of two components, one with a width of typically $\Delta\omega \approx 0.95°$ and an additional much narrower peak ($\Delta\omega \lesssim 0.1°$). A similar profile has been found for single Nb films on sapphire.[14,16] The x-ray data can be explained by a grain structure containing a bimodal distribution of columns and fine equiaxed grains in between. The aligned growth in the (110) direction persists also at low temperatures because it is determined by the early stages of growth on the substrate. The grain structure of the samples determines the low-temperature resistivity (Sec. III D) and is probably responsible for a broadening of SC transitions in magnetic fields as discussed in Sec. IV B 1.

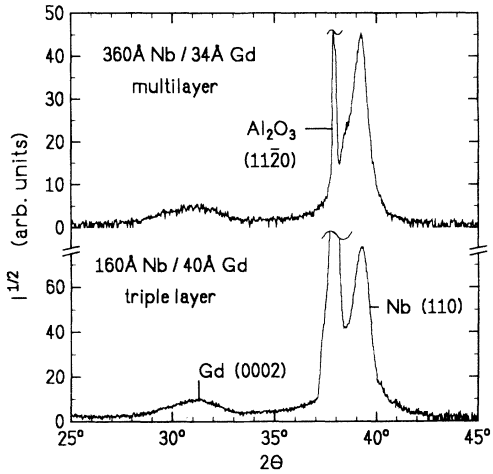

FIG. 1. Square root of x-ray scattering intensity vs scattering angle 2θ of Nb and Gd in a multilayer (upper panel) and a triple layer sample (lower panel).

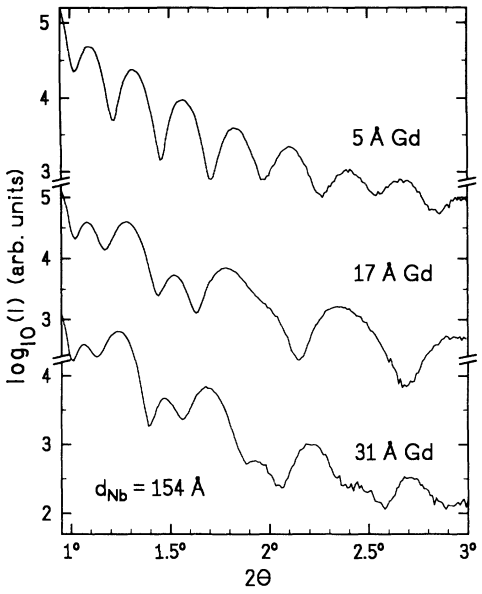

FIG. 2. Small-angle scattering intensity I (logarithmic) vs scattering angle 2θ for three samples of a triple layer series, prepared in a single evaporation run.

Figure 2 shows the small-angle scattering data of three samples taken from a series of Nb 154 Å/Gd X/Nb 154 Å triple layers produced in a single run as described above. The large number of observed reflections indicates the formation of sharp and parallel boundaries with only a small fluctuation of the layer thickness. From the distance of the interference maxima, the total layer thickness can be easily obtained, with the appropriate correction of the effect of refraction at small angles.[11] The difference between the total layer thickness of "first" and "last" sample of a series gives the total variation of d_{Gd} within that series and agrees well with the nominal total thickness obtained with the quartz monitors. While the thinnest sample ($d_{Gd}=5$ Å) appears as a homogeneous scatterer, the layered structure of the samples becomes visible in the variation of intensities of the peaks with increasing separation of the Nb films by the Gd interlayer. Because the two Nb sublayers are of approximately half of the total thickness, every second peak is depressed, compared to the sample with $d_{Gd}=5$ Å.

B. Reflection high-energy electron diffraction (RHEED)

The small thickness impedes the sufficient characterization of the Gd interlayers by x-ray diffraction. Because of the strong influence of the Gd interlayers on the SC properties of the samples, their growth has been studied further by RHEED. The RHEED patterns, recorded during evaporation, provide additional information about the growth mode of Gd on Nb. Figure 3(a) shows the results for a Nb buffer layer on sapphire, deposited at a high temperature $T_S=750°$ C (unlike the other samples of this work). Besides the streaks typical for smooth growth some weak bulklike diffraction spots are visible, indicating the presence of a small surface roughness. The distance between adjacent streaks corresponds to a lattice parameter of $d=1.65$ Å, indicating the direction of the incident electron beam (azimuth) along $[\bar{1}10]$. After deposition of nominally one monolayer of Gd ($T_S=80$ °C), an additional line appears [Fig. 3(b)], which can be attributed to the Gd lattice planes (azimuth $[\bar{1}010]$, lattice parameter $d=1.82$ Å). The coexistence

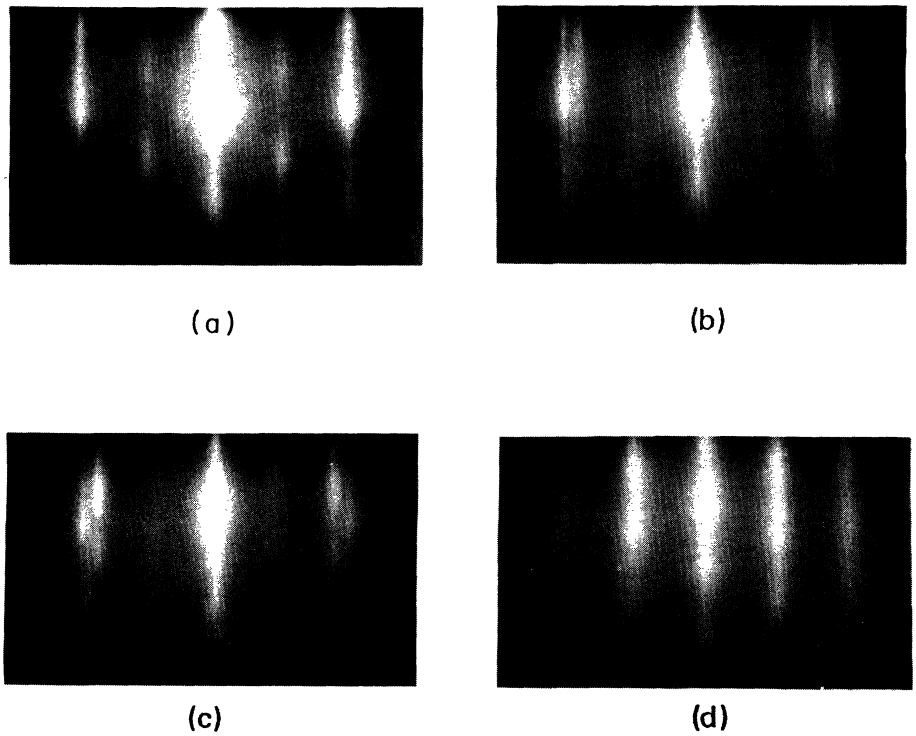

FIG. 3. RHEED patterns of Gd on Nb (110) for different nominal thicknesses of Gd: (a) Nb buffer layer ($T_S=750$ °C), (b) 3-Å Gd, (c) 5-Å Gd, (d) 13-Å Gd.

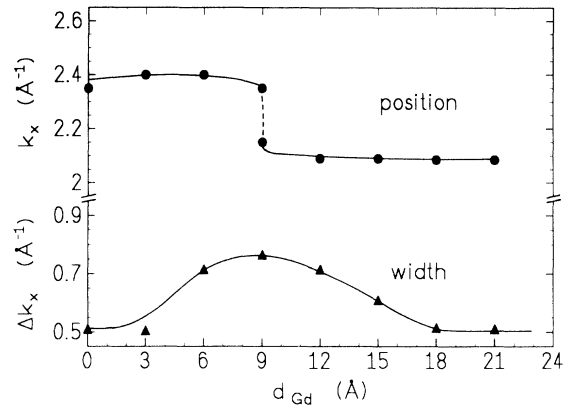

FIG. 4. Changes in position (upper panel) and width (lower panel) of RHEED reflections during evaporation of Gd onto a Nb buffer layer ($T_S = 25\,^\circ$C). The lines are guides to the eye.

of both lines indicates that the Gd layer grows initially in an island mode. After deposition of nominally 5-Å Gd the Nb streaks fade [Fig. 3(c)], indicating a reduction of the uncovered area of the Nb film. At a thickness of nominally 13-Å Gd only the Gd lines remain, Fig. 3(d) azimuth [11$\bar{2}$0]. Beyond this thickness smooth epitaxial growth of Gd has been achieved, though the width of the streaks reflects the small grain size obtained at low evaporation temperature. If the Gd film is condensed onto a Nb buffer evaporated at room temperature, the resulting streaks are too broad to be distinguished on the RHEED screen, possibly due to the higher disorder in the films. However, measurements of the RHEED profile, i.e., the streak position and its width yield the same information (Fig. 4). We find a shift of the streak position from Nb (azimuth [$\bar{1}$11]) to Gd (azimuth [11$\bar{2}$0]) at $d_{Gd} \approx 9$ Å, while the width reaches its initial value at about 20 Å. We conclude that the formation of a continuous Gd film on a Nb buffer evaporated at 750 °C starts around $d_{Gd} \approx 13$ Å and around $d_{Gd} \approx 18$ Å if the Nb buffer layer is deposited at 25 °C.

C. Magneto-optical Kerr effect

The saturation magnetization of Gd is dominated by the contribution of the 4f moments.[9] Thus, it is a direct measure for the strength of the exchange field due to the ordered 4f moments that gives rise to a Zeeman splitting of the conduction-electron band. According to the theory,[6] this splitting governs the breaking of Cooper pairs in the FM layers. Measurements of the magnetization of the Gd films have been performed using the transverse magneto-optical Kerr effect.[17] Detailed investigations show that Gd films ($T_S = 300\,^\circ$C), which are evaporated onto a Nb (110) buffer layer ($T_S = 750\,^\circ$C), order magnetically down to $d_{Gd} \approx 15$ Å with T_{Curie} decreasing with d_{Gd}, while in films with $d_{Gd} = 11$ Å and $d_{Gd} = 12$ Å no ferromagnetic signal was found.[17] The critical thickness for the formation of a FM-ordered film increases to 15 Å $< d_{Gd} <$ 20 Å when preparing the whole sample at room temperature, i.e., under the same conditions as the superconducting samples in this work. In the latter case, the Curie temperatures reduce to 140, 220, and 255 K for $d_{Gd} = 20$, 25, and 34 Å, respectively. This reduction is partly due to the decrease of the FM exchange field with smaller number of nearest neighbors in the thinner films. The number of nearest neighbors decreases further if the films become inhomogeneous. No ferromagnetic hysteresis has been found in a 15-Å Gd sample. The saturation magnetization (in $B_{ext} = 100$ mT) shows a similar decrease with decreasing d_{Gd}. Thus, in the island growth mode the ferromagnetic order breaks down completely. This structure-induced change in the magnetic properties is reflected in the superconducting properties, too, as will be one of the main topics of this work.

D. Electrical resistivity

A further characterization of the sample quality is the electrical resistivity. The resistance in each layer is governed by the following scattering processes: (i) electron-phonon scattering, (ii) scattering at dislocations, point defects and grain boundaries, and (iii) scattering at the layer boundaries. If the scattering processes are independent, the contributions to the resistance are additive (Matthiessen's rule). This is not the case for the scattering at grain boundaries and interface boundaries.[18] For our structures the contribution of the Gd layers to the total conductance can be neglected, because they are much thinner than the Nb layers. This is demonstrated in Fig. 5, which shows that the low-temperature resistivity $\rho_0 = \rho(10\text{ K})$ of several triple-layers series as a function of d_{Gd} is essentially constant. The scatter of the data points is determined by the error in the geometry factor only, because the Nb layers are identical within each series. Figure 6 shows the dependence of ρ_0 on d_{Nb} of single, triple, and multilayer samples. For 180 Å $\lesssim d_{Nb} \lesssim$ 1500 Å, we obtain $\rho_0 \sim 1/d_{Nb}$, while at lower d_{Nb} an additional increase can be seen. The surface scattering according to the Fuchs-Sondheimer theory[19]

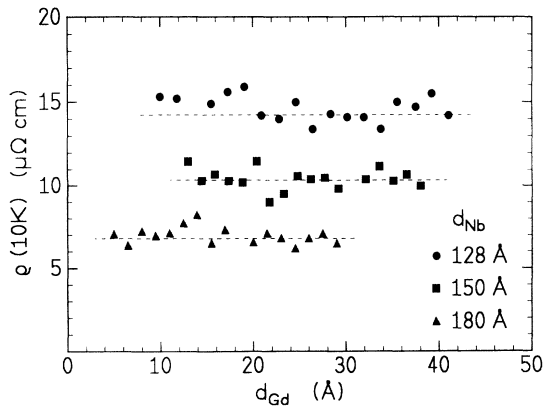

FIG. 5. Low-temperature resistivity ρ (10 K) as a function of d_{Gd} of several triple layer series, prepared in a single evaporation run. The dashed lines are guides to the eye.

TABLE I. Material parameters and characteristic lengths of different types of samples.

Sample type	Single layer		Triple layer			Multilayer		
d_{Nb} (Å)	190	1500	188	259	350	360	500	700
ρ_0 ($\mu\Omega$ cm)	6.7	1.8	6.1	5.6	4.2	3.8	4.0	2.6
T_c (K)	8.57	8.76	3.18	5.30	6.95	3.23	5.59	7.49
l_{eff} (Å)	57	215	63	67	92	100	96	150
ξ_S from ρ_0 (Å)	76	104	78	81	90	94	92	108
ξ_S from $H_{c2\perp}$ (Å)	72	93	79.5	88	82	79.5	86	88
ξ_S from $H_{c2\parallel}$ (Å)		110				81	87	91

yields a straight line for ρ_0 vs $1/d_{Nb}$ with a slope given for Nb by the constant $C_{Nb}=(\rho_0 \cdot l)_{bulk}=3.75\times10^{-16}$ Ωm^2,[20] where l is the intrinsic elastic mean free path. The effective mean free paths in the Nb films, determined from $C_{Nb}=\rho_0 \cdot l_{eff}$, are listed in Table I. Even for diffuse scattering the theoretical resistivity is much smaller than the experimental data (dashed line in Fig. 6). Grain boundaries provide a further source of electron scattering, which can be taken into account by use of the model of Mayadas and Shatzkes.[18] The assumption that the mean grain size is roughly proportional to d_{Nb} (a behavior which is often found in thin films[21]) allows one to fit the Mayadas-Shatzkes curve to the data above $d_{Gd}\approx200$ Å. Figure 6 additionally displays the resistivity of a single 250-Å Nb layer, which was evaporated at 750 °C. This data point lies nearly on the Fuchs-Sondheimer line, in accordance with the epitaxial growth obtained for this high deposition temperature.[14,22] For $d_{Nb}\lesssim180$ Å the strong scattering of the data points indicates the increasing influence of the individual microstructure of the films. In particular, the roughness of the Nb/Gd interface may give rise to a more pronounced electron scattering at low d_{Nb}.

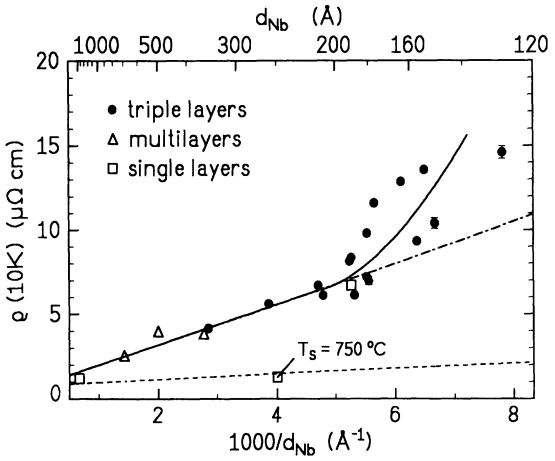

FIG. 6. Low-temperature resistivity ρ (10 K) as a function of d_{Nb}^{-1} for different types of layer structures. The error bars denote the statistical error, which has been determined from the series in Fig. 5. The full line is a guide to the eye, the dash-dotted lines a fit according to the Mayadas-Shatzkes theory, and the dashed line a fit according to the Fuchs-Sondheimer theory.

IV. PAIR BREAKING BY THE PROXIMITY EFFECT AND EXTERNAL MAGNETIC FIELDS: DEPENDENCE OF T_c AND H_c ON d_{Nb}

We first present the results emerging from the variation of d_{Nb}, while d_{Gd} has been kept constant at 34 Å. In this series of measurements we compare the behavior of triple and multilayers in the regime were the Gd layers are ferromagnetic.

A. Transition temperatures

The SC transition temperatures have been determined from the midpoint of the resistive (ρ) and the diamagnetic (χ) transitions (Fig. 7). With decreasing d_{Nb}, T_c shows

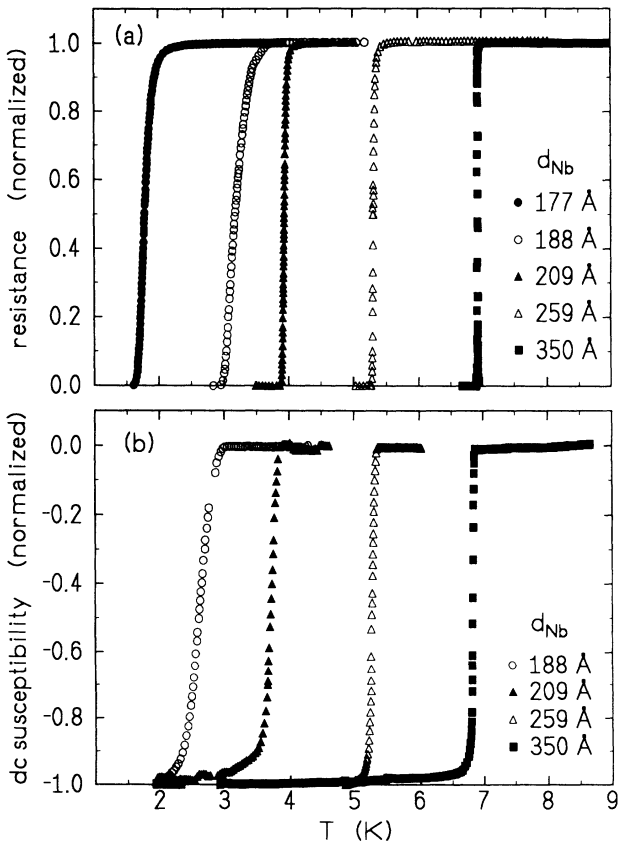

FIG. 7. Resistance (a) and dc susceptibility (b) of as a function of temperature of triple layers at constant $d_{Gd}=34$ Å.

a continuous depression down to a critical thickness d_c (Fig. 8). Both methods yield the same T_c for large d_{Nb}, while for $d_{Nb} \lesssim 200$ Å, T_c^χ is somewhat lower than T_c^ρ. Because of the steep decrease of $T_c(d_{Nb})$ near the critical thickness d_c, T_c^ρ becomes very sensitive to any inhomogeneity of the sample (for instance fluctuations of d_{Nb}), which gives rise to superconducting percolation paths above T_c. Therefore, T_c^χ, which is determined from a bulklike measurement, lies always somewhat below T_c^ρ.

The decrease of T_c is caused by the depression of the SC pair amplitude F_S near the SC/FM boundary due to the proximity effect. Single Nb layers of comparable thickness show only minor T_c depressions due to disorder as reflected by the electrical resistivity (see Table I and Refs. 14, 23). In the Nb layers of the triple layer configuration the Cooper pairs are subjected to the pair breaking at one boundary only, while in the multilayer configuration F_S is depressed at both boundaries, resulting in a much stronger T_c depression. Due to a simple symmetry argument, $T_c(d_{Nb})$ for both configurations should fall on a common curve, if d_{Nb} is scaled by a factor of 2. This argument still holds in presence of a perpendicular magnetic field but breaks down in presence of a parallel magnetic field, where the influence of surface superconductivity is expected (see Sec. IV B and Ref. 24). Although T_c of the multilayers is somewhat higher than T_c of triple layers of corresponding thickness, the qualitative agreement supports the simple symmetry argument (Fig. 8).

According to a recent Ginzburg-Landau (GL) theory,[25] T_c of an SC film of thickness d_{Nb} sandwiched between FM layers is given by

$$d_{Nb} = \frac{\pi \xi_S}{\sqrt{t_c}} \arctan(b + a/\sqrt{t_c})^{1/2} \quad \text{with } t_c = (T_{c0} - T_c)/T_{c0} \qquad (1)$$

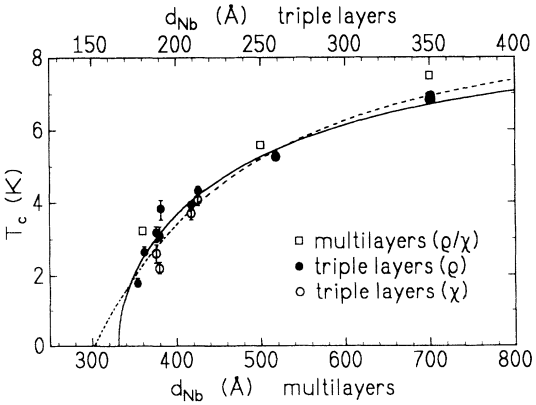

FIG. 8. Resistively (ρ) and inductively (χ) determined transition temperatures T_c of triple layers and multilayers as a function of d_{Nb}. d_{Gd} was kept constant at 34 Å. Note that the d_{Nb} axis for triple layers and multilayers differ by a factor of 2. The bars denote the 10–90% transition widths, if it is larger than the dot size. The solid line is a fit according to the Radovic theory, and the dashed line according to the theory of Schinz and Schwabl.

where T_{c0} is the SC transition temperature without pair breaking at the interfaces and ξ_S is the SC coherence length related to the GL coherence length by $\xi_{GL} = (\pi/2)\xi_S(1 - T/T_{c0})^{-1/2}$, and a, b are parameters related to the coupling between the SC and FM order parameters and the interface properties. a and b can be related to microscopic parameters[26] and have for Nb and Gd the values $a = 7.25$ and $b = 4 \times 10^{-4}$.[27] A best fit of Eq. (1) to our data yields the dashed line in Fig. 8 with $a = 7.47$, $b = 0$ and $\xi_S = 78$ Å. As expected for a GL theory, the agreement between theory and experiment becomes worse at low T_c, i.e., near the critical thickness d_c. Also, the fit implies that the surface parameter η (see below) is equal to the conductivity ratio σ_M/σ_S of FM and SC layers, contrary to what we analyze below. In any case, the value of ξ_S is in good agreement with the one determined independently from the resistivity and the perpendicular critical field of a single 190-Å Nb film evaporated under identical conditions. ξ_S has been calculated from the resistivity using[28]

$$\xi_S = 0.470 \left[\frac{\xi_{BCS} R(\lambda_{tr})}{\xi_{BCS}^{-1} + 0.882 l_{eff}^{-1}} \right]^{1/2},$$

where $\xi_{BCS} = 0.180 \hbar v_F / k_B T_{c0} = 420$ Å with $v_F = 2.77 \times 10^7$ cm/sec (Ref. 20) and $T_{c0} = 8.57$ K. The quantity $R(\lambda_{tr})$ is similar to the Gorkov χ function.[29] It depends weakly on the mean free path via the ratio $\lambda_{tr} = 0.882 \xi_{BCS}/l_{eff}$ and in our samples has the value 1.06 ± 0.03.

The microscopic theory by Radovic *et al.*[6] considers multilayers in the case of completely decoupled SC films in the dirty limit, i.e., $d_{FM} \to \infty$. Our films satisfy both requirements. As will be shown in Sec. V, the effect of Gd interlayers has nearly saturated at $d_{Gd} = 34$ Å. The critical temperature T_c is governed by the pair-breaking parameter ρ via the familiar equation

$$\ln\left(\frac{T_c}{T_{c0}}\right) = \Psi\left(\frac{1}{2}\right) - \mathrm{Re}\,\Psi\left(\frac{1}{2} + \rho\frac{T_{c0}}{T_c}\right), \qquad (2)$$

where Ψ is the digamma function. ρ can be calculated from the solution of Usadel's equations for the pair amplitude F_S.[6] It depends on d_{Nb} and two material parameters, namely the coherence length ξ_S and $g = \xi_M/\eta$, the ratio between the penetration depth of Cooper pairs into the FM and a coefficient η stemming from the (generalized) DGWH boundary condition in Ref. 6:

$$\frac{\partial}{\partial x} \ln F_S \Big|_{\text{boundary}} = \eta \frac{\partial}{\partial x} \ln F_M \Big|_{\text{boundary}}.$$

F_S and F_M denote the pair amplitude in the SC and the FM layer, respectively. By fitting the theoretical curve (full line in Fig. 8) to the data, we obtain $\xi_S = (78 \pm 5)$ Å and $g = (235 \pm 10)$ Å. ξ_M and η cannot be determined independently from the experiment, but may be estimated using $\xi_M = \sqrt{4\hbar D_M/I_0}$ where D_M is the electron diffusion constant in the FM layers and $2 \cdot I_0$ the splitting of the Gd spin-up and spin-down conduction (sub)bands by the exchange field of the ordered $4f$ moments. As dis-

cussed in Sec. III D, the mean free path in the Gd layers and consequently $D_M=(1/3)\cdot v_F l_M$ cannot be extracted from the total resistivity of the samples. We therefore assume $l_M \approx d_{Gd}$, which is reasonable because the scattering at interlayer boundaries should dominate the mean free path in films of such a small thickness. Because D_M enters ξ_M under the square root only, this assumption is not very critical. Using $v_F=1.17\times10^7$ cm/sec (Ref. 30) we obtain $D_M=1.3$ cm^2/sec for $d_{Gd}=34$ Å. I_0 in the films with $d_{Gd}=34$ Å is probably somewhat reduced with respect to the bulk value as inferred from the reduction of T_{Curie}. Using $2\cdot I_0=0.61$ eV as experimentally determined for bulk Gd,[31] we get $\xi_M \approx 11$ Å. Together with the above value of g we have $\eta \approx 0.047$. This value is considerably smaller than the DGWH value $\eta=0.33$, i.e., the ratio of normal-state conductivities, which should be valid for specular scattering at the SC/NC boundaries (NC: nonmagnetic normal conductor). This could be interpreted by assuming that the jump in the logarithmic derivative of the pair amplitude is enhanced, i.e., the decoupling of F_S and F_M across the boundary becomes stronger in case of diffuse scattering. On the other hand, it is not yet known whether there is a difference between the microscopic boundary conditions at SC/NC interfaces and SC/FM interfaces.[6] Therefore, Radovic *et al.* have treated η as a phenomenological parameter. Using $\eta=\sigma_M/\sigma_S \approx 0.33$ would give $\xi_M=g\cdot\eta=77$ Å, which is unreasonably high. This will be discussed further in Sec. V.

There also exists a more sophisticated version of the theory,[7] which includes the coupling of SC layers expected in the case of very thin FM layers. However, in our case the use of the simple version of the theory is sufficient, since the deviations of the calculated $T_c(d_{Nb})$ curve from the exact calculation are below 1%.[32]

B. Critical fields

Measurements of the perpendicular and parallel critical fields were performed to give additional information on the coherence length and the dimensionality of the samples. Moreover, they allow a consistency check of our results. Figure 9 shows the resistivity as a function of magnetic field of a Nb 350 Å/Gd 34 Å/Nb 350 Å triple layer. The broadening of the transition in higher fields appears in thick samples only and will be discussed below.

1. Perpendicular critical field

A perpendicular magnetic field gives just an additional contribution to the pair-breaking parameter ρ which is independent of d_{Nb}.[6] Therefore, the slopes of the perpendicular critical fields are progressively depressed with decreasing d_{Nb} (Fig. 10) much like T_c itself. Since the normal component of the magnetic induction B is always continuous at interfaces, the symmetry argument for T_c in triple layers and multilayers of corresponding thickness should hold also in this case. Apart from minor deviations, which are unavoidable for samples prepared in different runs, this is again confirmed by the experiment.

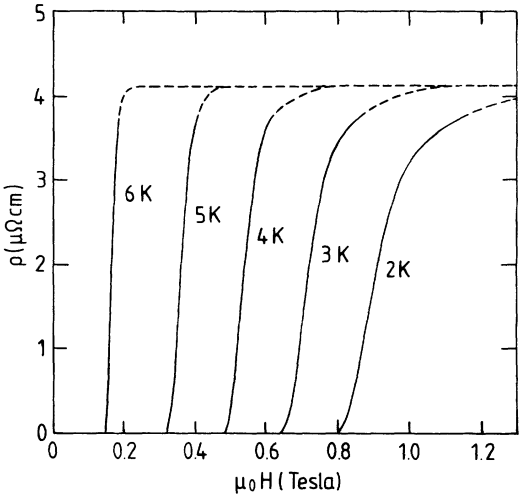

FIG. 9. Resistivity ρ as a function of perpendicular magnetic field for different temperatures of a Nb 350 Å/Gd 34 Å/Nb 350 Å triple sample. The dashed part of the curves has been extrapolated to the measured ρ (10 K). Because of the long high field end of the transitions, the last 10% of the transition were not measured.

Keeping $g=235$ Å fixed, the theoretical fits have been adjusted to the data by small variations of ξ_S (see Table I). These variations qualitatively reflect the increase of the mean free path with increasing d_{Nb} discussed above. The broadening of $H_{c2\perp}$ in the 700-Å multilayer and the 350-Å triple layer sample is a feature encountered in sin-

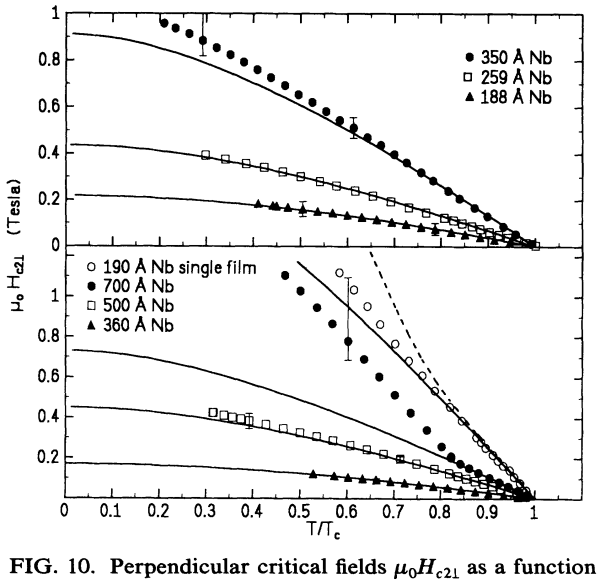

FIG. 10. Perpendicular critical fields $\mu_0 H_{c2\perp}$ as a function of reduced temperature T/T_c for triple layers (upper panel) and multilayers (lower panel). The bars denote the 10–90% width of the resistive transitions. The width in the 259-Å samples is about the size of the dots. Solid lines are theoretical curves as described in the text. Additionally, the magnetic fields corresponding to the 10% values (open circles) and the 90% values (dashed line) of the resistive transition in a 190-Å single Nb layer are shown.

gle Nb layers, too.[23] This effect is probably due to the grain structure of the Nb films. As discussed in Sec. III A, in samples of low substrate temperatures large, epitaxially oriented grains are connected by a transition region of smaller, slightly canted grains. These transition regions exhibit enhanced disorder, i.e., reduced conductivity and, for Nb, reduced transition temperature.[33] Following Zwicknagl and Wilkins,[34] a spatial fluctuation of the conductivity gives rise to an increasing broadening of the SC transition with increasing magnetic field. Because T_c is depressed by the disorder also, superconductivity appears at lower temperatures in the grain boundaries than inside the grains. This can be seen in the 190-Å single layer, in which the 10% (open circles in Fig. 10) and the 90% values of the resistive transition (dashed line in Fig. 10) lie close together above $T/T_c=0.8$, or 6.5 K. At lower temperatures, the fine-grained transition regions between the columns give rise to the broadening of the transition. The same explanation should hold for the upturn of $H_{c2\perp}$, observed in the 700-Å multilayer sample. Apparently, the proximity of the FM layers suppresses this effect at lower d_{Nb}.

2. *Parallel critical field*

In a parallel magnetic field the situation is complicated by several effects. The pair-breaking parameter is no longer additive but a more complicated function of the external and the exchange field.[6] Figure 11 shows the results for triple and multilayers and for a 1500-Å Nb layer. In the single layer, surface superconductivity is suppressed by evaporation of 100-Å Gd layers.

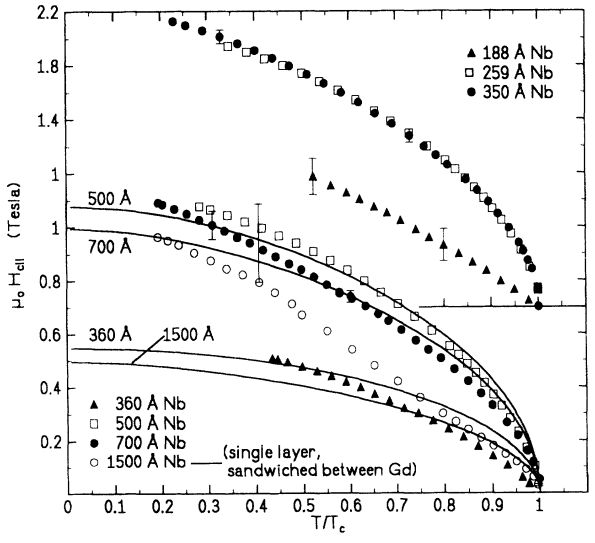

FIG. 11. Parallel critical fields $\mu_0 H_{c\parallel}$ as a function of reduced temperature T/T_c for triple layers (upper panel) and multilayers (lower panel). The bars denote the 10–90% width of the resistive transitions. The width of the 259-Å sample is about the size of the dots. Solid lines are theoretical fits described in the text. Additionally the data for a 1500-Å single Nb layer (sandwiched between 100-Å Gd) are shown. Because of the strong broadening of the transition in this sample, the 10% transition points have been used.

Because of the reduced dimensionality, a square-root dependence of $H_{c\parallel}(T)$ is expected near T_c.[35] This behavior is indeed found, except for the thinnest Nb films. Instead, these samples (188-Å triple layer and 360-Å multilayer) exhibit linear behavior near T_c, a property which is not yet understood. Further, as already mentioned, the analogy between triple layer and multilayer samples breaks down. In all samples, the parallel critical field of the triple layers is enhanced by a factor of about 1.9 with respect to the multilayers. This behavior can be explained by the nucleation of surface superconductivity at the free surface of the triple layers. An interesting feature is the nonmonotonic dependence of $H_{c\parallel}$ on d_{Nb}. At low d_{Nb}, $H_{c\parallel}$ increases with increasing d_{Nb}, as expected from the decreasing influence of the exchange field. Above $d_{\mathrm{Nb}}=500$ Å, $H_{c\parallel}$ decreases again, which is due to the growing orbital effect of the magnetic field. For small d_{Nb}, the orbital effect is small because here the London penetration depth is comparable to or larger than d_{Nb}. As in case of $H_{c2\perp}$, the theoretical curves for $H_{c\parallel}$ (solid lines in Fig. 11) are adjusted to the data by small variations of ξ_S (see Table I), while g has been kept constant at 235 Å. The slightly different values of ξ_S in the same sample resulting from the $H_{c2\perp}$ and the $H_{c\parallel}$ measurement are probably due to the different averaging of thickness fluctuations in both cases.

At higher temperatures, the theoretical curves show fair agreement with the experimental data, but for $T<0.5\times T_c$ the fits lie systematically too low. This behavior, appearing most pronounced in the 1500-Nb film, can be attributed to vortex nucleation, which is not included in the simple version of the theory that we have used. Further extensions of the theory show that vortex nucleation can in fact occur above a critical thickness which is considerably enhanced with respect to that of a single SC film in vacuum.[8] In the region of vortex nucleation, i.e., at low temperature and high field, the curves should approach each other, provided the thickness is sufficiently larger than d_c.[8] This is in fact observed, cf. the data for multilayers in Fig. 11.

The transition between vortex and laminar nucleation (in a certain sense a change of the effective dimensionality of the single Nb layers) causes no distinct structure in the $H_{c\parallel}$ curve. It has to be distinguished from the two-dimensional–three-dimensional crossover occurring additionally in NC/SC multilayers[35] [i.e., the upturn in the $H_{c\parallel}(T)$ curve], where near T_c the increasing penetration depth of Cooper pairs into the NC layers gives rise to a coupling of the SC layers of the structure. In this regime, the total layer thickness governs the dimensionality behavior of the sample. In SC/FM multilayers the latter effect is absent, due to the temperature-independent penetration depth of Cooper pairs into the ferromagnet, which is mainly determined by the strength of the exchange field.

V. MICROSCOPIC ORIGIN OF PAIR BREAKING: DEPENDENCE OF T_c ON d_{Gd}

In this section, the influence of the magnetic properties of the Gd layers on the SC transition temperatures is ad-

dressed. We have measured eight series of Nb/Gd/Nb layers keeping d_{Nb} constant within each series. The thickness of the top and bottom Nb layer has been chosen equal with exception of the 168-Å Nb series. Here the top layer ($d_{Nb}=50$Å $\ll d_c$, i.e., $T_c=0$) served just to protect the Gd layer against oxidation. Therefore, concerning the SC properties the samples of this series behave like bilayers. The experimental problem arising in measuring $T_c(d_{Gd})$ is that T_c depends on d_{Nb}/ξ_S also. In the most interesting region—near d_c—this dependence is most pronounced, because there $T_c(d_{Nb}/\xi_S)$ has the steepest slope. Thus, it was crucial to evaporate each series in a single run to obtain exactly identical properties of the Nb layers with same and ξ_S and well defined values of d_{Gd} as described in Sec. II.

The SC transition temperatures were measured resistively and showed a continuous depression with increasing d_{Gd} (Fig. 12). For the 191-Å Nb series, T_c was checked additionally by SQUID magnetometry.[15] Apart from a constant shift of 0.3 K, the T_c^X data follow exactly the $T_c^\rho(d_{Gd})$ curve which demonstrates the sample quality achieved. Depending on d_{Nb}, T_c saturates for large d_{Gd} or tends to zero. In series with d_{Nd} close to or below the critical thickness d_c the transitions broaden at high values of d_{Gd}, indicating again the increasing influence of inhomogeneities near d_c. Around $d_{Gd}=(20\pm5)$ Å a sudden drop appears in the curves. On each side of this step T_c shows a plateaulike flattening, especially in the series with 154, 168, and 191-Å Nb.

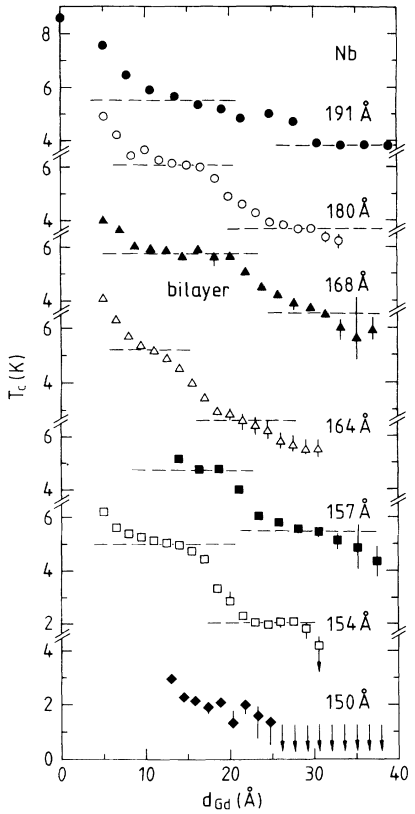

FIG. 12. Resistively determined transition temperatures T_c as a function of d_{Gd} in several series of triple layers that have been prepared in a single evaporation run. The bars denote the 10–90 % transition width, if it is larger than the dot size. The dashed line correspond to the plateau values of the T_c reduction displayed in Fig. 13.

As suggested by the structural and magnetic characterization of the Gd films (Secs. III B and III C) we attribute this structure to the onset of long-range ferromagnetic order. In Fig. 13 we plot the T_c reductions $(T_{c0}-T_c)/T_{c0}$ found on both sides of the step (corresponding to the dashed lines in Fig. 12) as a function of d_{Nb}. This comparison of the paramagnetic and the ferromagnetic regime shows directly the much more effective pair breaking in the latter. In the paramagnetic (PM) range ($d_{Gd}\lesssim 20$ Å), spin-flip scattering should give the dominant contribution to the pair breaking at the SC/FM boundary. A first indication of such an effect was observed by Moodera and Meservey, in the system Pb/Ni with an rf inductance method.[36]

Following Hauser *et al.*,[4] the transition temperature is given again by Eq. (2), where the pair-breaking parameter reads

$$\rho(T)=\tfrac{1}{2}\xi_S^2\cdot k_S^2(T)\ .$$

k_S which is a measure of the inverse length scale on which the SC order parameter changes, can be calculated from the DGWH boundary condition, which reads in case of the Werthamer approximation (i.e., assuming simple exponential decay of F_M),[37]

$$k_S\tan k_S d_{Nb}=\eta k_M\tanh k_M d_{Gd}/2\ .$$

The dashed line in Fig. 13 was obtained by fitting the DGWH-AG theory to the data yielding k_M^{-1}, and using $\xi_S=78$ Å and $\eta=0.047$ as determined from the $T_c(d_{Nb})$ curve in Fig. 8. This procedure yields $k_M^{-1}=(8.2\pm0.5)$ Å. [In the limit of strong spin-flip scattering (which is certainly fulfilled in the samples with low d_{Gd}) the penetration depth of Cooper pairs into the Gd layer k_M^{-1} is temperature independent.] To extract a spin-flip scattering time τ_{sf} requires knowledge whether the transport on this length scale is diffusive or ballistic (i.e., $k_M^{-1}=\sqrt{D_M\cdot\tau_{sf}}$ or $k_M^{-1}=v_F\cdot\tau_{sf}$). The dirty-limit theories

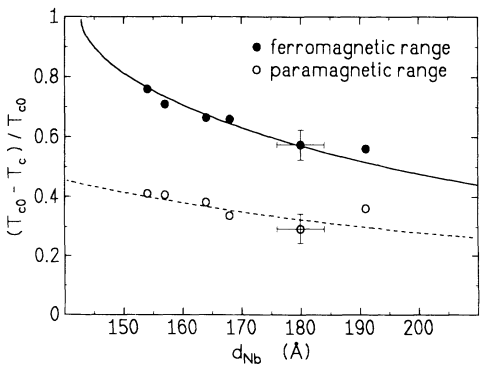

FIG. 13. T_c reduction in the ferromagnetic and the paramagnetic range as a function of d_{Nb}. The solid line corresponds to the Radovic theory, the dashed line to the DGWH-AG theory.

assume diffusive transport. In our case the resulting spin-flip scattering times in both regimes differ only insignificantly, with $\tau_{sf}=8.6\times10^{-15}$ sec and $\tau_{sf}=7\times10^{-15}$ sec, respectively.

Hauser, Theurer, and Werthamer[4] have always used $\eta=\sigma_M/\sigma_S$ in their analysis. As pointed out in Sec. IV A, this would give unreasonably high values for ξ_M. Using $\eta=\sigma_M(d_{Gd}=20\ \text{Å})/\sigma_S=0.19$ (as opposed to $\eta=0.047$) would yield $k_M^{-1}=19$ Å, which again is somewhat higher than our above value.

With the evolution of FM order, the spin-flip scattering time τ_{sf} increases by several orders of magnitude, because at low temperatures single Gd spins can hardly be flipped against the exchange field of their surrounding. In the limit of fully established ferromagnetism τ_{sf} is dominated by the scattering of magnons and diverges as T goes to zero.[38] In turn, the electron magnon scattering contributes to the magnon lifetime τ_m. Hence, a lower bound of τ_{sf} is approximately given by τ_m (neglecting other, probably even dominating, contributions to τ_m^{-1}). Measurements of the magnon linewidth ΔE by inelastic neutron scattering in bulk Gd (Ref. 39) gave at 4 K, $\tau_m^{-1}\approx\Delta E/h\approx0.1$ THz. Hence τ_{sf} would be larger than 10^{-11} sec. In contrast, fitting the data in the ferromagnetic range with the DGWH-AG theory requires an even reduced spin-flip scattering time of $\tau_{sf}=2.8\times10^{-15}$ sec with respect to the PM range, and hence makes this interpretation inappropriate in the FM regime.

Therefore, in the FM range ($d_{Gd}\gtrsim20$ Å) another pair-breaking mechanism must be present. This is most likely the depairing by the exchange splitting of the Gd conduction bands, treated in the theory of Radovic *et al.*,[6] which we employed in Sec. IV. Using again $\xi_S=78$ Å and $\eta=0.047$ the fit to the data in the FM regime gives together with $k_M=(1+i)\cdot2/\xi_M$ and $\xi_M=\sqrt{4\hbar D_M/I}$, the result $\xi_M=13.7$ Å (solid line in Fig. 13). The complex value for k_M reflects the nonmonotonic decay of the SC order parameter in the ferromagnet.

The estimate for the mean free path $l_M\approx20$ Å gives a somewhat lower $D_M=0.78$ cm^2/sec compared to 1.3 cm^2/sec at $d_{Gd}=34$ Å. Accordingly, we obtain $2I=0.22$ eV for the exchange splitting near the PM/FM boundary at $d_{Gd}\approx20$ Å, which is 35% of I_0 for Gd films with $d_{Gd}=34$ Å.[40] This demonstrates again the reduction of the FM exchange field at the PM/FM transition and is in qualitative agreement with the results of Sec. III C. In our analysis we have avoided the simultaneous variation of all three relevant parameters by assuming $\xi_S=78$ Å and $\eta=0.047$ to be appropriate mean values in all series of samples. Of course ξ_S and η differ somewhat in the different series as evident from the large scattering of the residual resistance ρ_0 (see Fig. 6).

A more detailed analysis would require an individual fitting of each $T_c(d_{Gd})$ curve. This could be done on the PM side but is difficult on the FM side. There are two possible reasons for the decrease of T_c with increasing d_{Gd} in the FM regime: (i) the increasing decoupling of the SC films by the increasing FM spacing, and (ii) the gradual establishment of the FM exchange field through the increasing homogeneity of the Gd layer.

While the first mechanism can probably be accounted for by the extended version of the theory of Radovic *et al.*,[7] the latter can hardly be described quantitatively.

VI. SUMMARY

We have investigated the interplay of magnetism and superconductivity in layered structures of Nb and Gd. Triple layers and multilayers with well-defined material parameters have been prepared. The dependence of the transition temperature and of the perpendicular critical fields on d_{Nb} has been explained quantitatively. A nonmonotonic variation of the parallel critical fields was observed as predicted theoretically.

With increasing thickness of the Gd layers, a structure-induced transition from PM to FM behavior was found. We have detected this transition also in the superconducting properties of the samples, which allows a direct comparison of the efficiency of the underlying pair-breaking mechanisms. The corresponding microscopic parameters have been determined by fitting the DGWH-AG for spin-flip pair breaking and a recent theory for exchange-field pair breaking to the data.

No evidence for the theoretically predicted oscillations in $T_c(d_{Gd})$ has been found so far. This might be due to the very short penetration depth of Cooper pairs into the ferromagnet which has been extracted from the experiment.

ACKNOWLEDGMENTS

We would like to thank Z. Radovic, L. Dobrosavlevic-Grujic, H. Schinz, and F. Schwabl for communicating their results prior to publication and providing some fits of their theories to the data. Further we thank K. Röhberg and T. Leverenz for supporting measurements, F. Baumann for helpful discussions and the Deutsche Forschungsgemeinschaft for financial support.

[1] P. Fulde and R. A. Ferrell, Phys. Rev. **153**, 550 (1964); A. I. Larkin and Yu. N. Ovchinnikov, Zh. Eksp. Teor. Fiz. **47**, 1136 (1964) [Sov. Phys. JETP **20**, 762 (1965)].

[2] D. St. James, G. Sarma, and E. J. Thomas, *Type-II Superconductivity*, (Pergamon, Oxford, 1969), Sec. 61.

[3] K. Gloos, R. Modler, H. Schimanski, C. D. Bredl, C. Geibel, F. Steglich, A. I. Buzdin, N. Sato, and T. Komatsubara, Phys. Rev. Lett. **70(4)**, 501 (1993).

[4] J. J. Hauser, H. C. Theurer, and N. R. Werthamer, Phys. Rev. **142**, 118 (1965).

[5]R. O. Smith, W. L. McLean, and B. Serin, J. Low Temp. Phys. **4**, 317 (1971); H. K. Wong, B. Y. Yin, H. Q. Yang, J. B. Ketterson, and J. E. Hilliard, J. Low Temp. Phys. **63**, 307 (1986).
[6]Z. Radovic, L. Dobrosavljevic-Grujic, A. I. Buzdin, and J. R. Clem, Phys. Rev. B **38**, 2388 (1988).
[7]Z. Radovic, L. Dobrosavljevic-Grujic, A. I. Buzdin, and J. R. Clem, Phys. Rev. B **44**, 759 (1991).
[8]M. Ledvij, L. Dobrosavljevic-Grujic, Z. Radovic, and J. R. Clem, Phys. Rev. B **44**, 859 (1991).
[9]W. C. Koehler, in *Magnetic Properties of Rare Earth Metals,* edited by R. J. Elliott (Plenum, New York, 1972), p. 81.
[10]J. Kwo, M. Hong, and S. Nakahara, Appl. Phys. Lett. **49**, 319 (1986).
[11]C. Sürgers and H. v. Löhneysen, Thin Solid Films **219**, 69 (1992).
[12]R. P. Elliot, *Constitution of Binary Alloys,* (McGraw-Hill, New York, 1965), First supplement, p. 256; F. A. Shunk, *Constitution of Binary Alloys* (McGraw-Hill, New York, 1969), Second supplement, p. 184.
[13]C. Strunk, C. Sürgers, K. Röhberg, and H. v. Löhneysen, in *Proceedings of the XXth International Conference on Low Temperature Physics,* edited by R. J. Donnelly, Physica B (to be published); C. Strunk, U. Paschen, C. Sürgers, and H. v. Löhneysen, *ibid.*
[14]C. Sürgers, C. Strunk, and H. v. Löhneysen, Thin Solid Films (to be published).
[15]K. Röhberg, Diploma thesis, University Karlsruhe, 1992.
[16]P. M. Reimer, H. Zabel, C. P. Flynn, and J. A. Duras, Phys. Rev. B **45**, 11 426 (1992).
[17]U. Paschen, C. Sürgers, and H. v. Löhneysen, Z. Phys. B **90**, 289 (1993).
[18]A. F. Mayadas and M. Shatzkes, Phys. Rev. B **1**, 1382 (1970).
[19]E. H. Sondheimer, Adv. Phys. **1**, 1 (1952).
[20]H. W. Weber, E. Seidl, C. Laa, E. Schachinger, M. Prohammer, A. Junod, and D. Eckert, Phys. Rev. B **44**, 7585 (1991).
[21]J. R. Sambles, Thin Solid Films **106**, 321 (1983).
[22]C. Sürgers, Ph.D. thesis, University Karlsruhe, 1991.
[23]C. Strunk, Ph.D. thesis, University Karlsruhe, 1992.
[24]W. Maij and J. Aarts, Phys. Rev. B **44**, 7745 (1991).
[25]H. Schinz and F. Schwabl, J. Low Temp. Phys. **88**, 347 (1992).
[26]H. Suhl, J. Less. Common Met. **62**, 225 (1977).
[27]H. Schinz (private communication).
[28]T. P. Orlando, E. J. McNiff, S. Foner, and M. R. Beasley, Phys. Rev. B **19**, 4545 (1979).
[29]N. R. Werthamer, in *Superconductivity Vol. I,* edited by R. D. Parks (Dekker, New York, 1969), p. 339.
[30]T. Kasuya, in *Magnetism Vol. IIb,* edited by G. T. Rado and H. Suhl (Academic, New York, 1966).
[31]A. J. Freeman, in *Magnetic Properties of Rare Earth Metals,* edited by R. J. Elliott (Plenum, New York, 1972), p. 311.
[32]L. Dobrosavljevic-Grujic (private communication).
[33]S. I. Park and T. H. Geballe, Physica **135B**, 108 (1985).
[34]G. Zwicknagl and J. W. Wilkins, Phys. Rev. Lett. **53**, 1276 (1984).
[35]S. T. Ruggiero and M. R. Beasley, in *Synthetic Modulated Structures,* edited by L. L. Chang and B. C. Giessen (Academic, London, 1985), and references therein.
[36]J. S. Moodera and R. Meservey, Phys. Rev. B **34**, 379 (1986).
[37]G. Deutscher and P. G. DeGennes, in *Superconductivity Vol. II,* edited by R. D. Parks (Dekker, New York, 1969), p. 1013.
[38]A. R. Mackintosh and H. B. Moller, Ref. 31, p. 236; I. A. Campbell and A. Fert, in *Ferromagnetic Materials Vol. 3,* edited by E. P. Wohlfahrt (North-Holland, Amsterdam, 1982).
[39]J. W. Cable, R. M. Nicklow, and R. M. Wakabashi, Phys. Rev. B **32**, 1710 (1985).
[40]In a recent paper [B. Kim, A. B. Andrews, J. L. Erskine, K. J. Kim, and B. N. Harmon, Phys. Rev. Lett. **68**, 1931 (1992)], the exchange splitting of the Gd conduction band was determined to be $I_0=0.85$ eV instead of the earlier value 0.61 eV (Ref. 31). The slight changes of $\xi_M \sim I_0^{-1/2}$ and η do not affect our main results and conclusions.

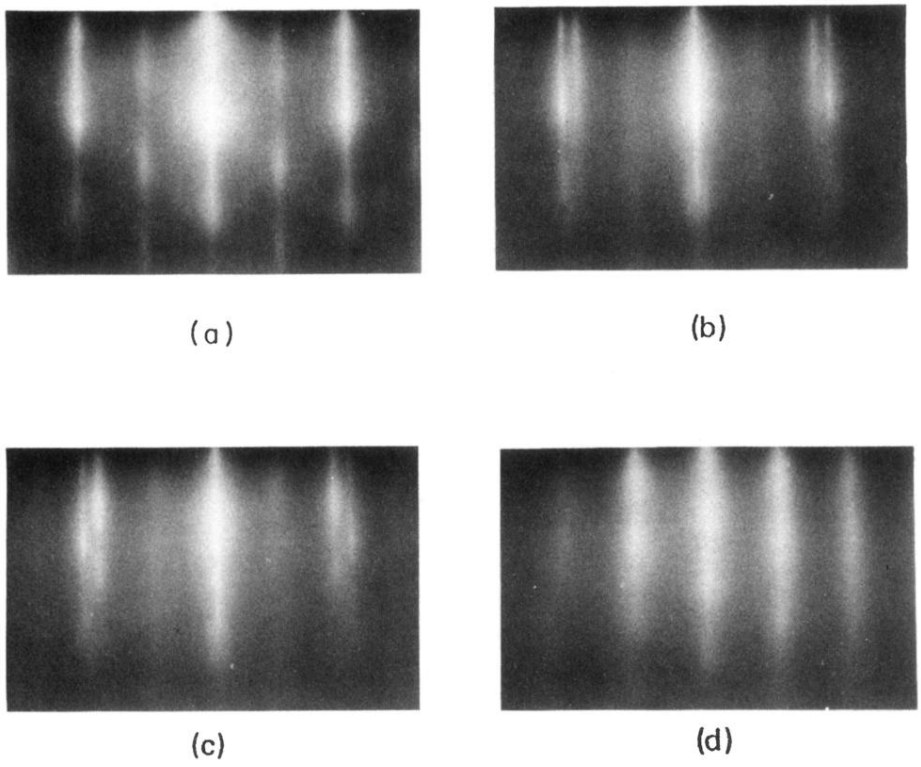

FIG. 3. RHEED patterns of Gd on Nb (110) for different nominal thicknesses of Gd: (a) Nb buffer layer ($T_S = 750\,^{\circ}\mathrm{C}$), (b) 3-Å Gd, (c) 5-Å Gd, (d) 13-Å Gd.